arXiv:1604.06779v1 [astro-ph.HE] 22 Apr 2016

Near-Infrared Spectroscopy of Faint Discrete X-ray Point Sources Constituting the Galactic Ridge X-ray Emission

Kumiko MORIHANA[1], Masahiro TSUJIMOTO[2], Pierre DUBATH[3], Tessei YOSHIDA[4], Kensuke SUZUKI[5], and Ken EBISAWA[2]

[1]Nishi-Harima Astronomical Observatory, Center for Astronomy, University of Hyogo, 407-2 Nichigaichi, Sayo-cho, Sayo, Hyogo, 670-5313

[2]Japan Aerospace Exploration Agency, Institute of Space and Astronautical Science, 3-1-1 Yoshino-dai, Chuo-ku, Sagamihara, Kanagawa 252-5210

[3]Department of Astronomy, University of Geneva, 16 Ch. d'Ecogia, 1290, Versoix, Switzerland

[4]National Astronomical Observatory of Japan, 2-21-1 Osawa, Mitaka, Tokyo, 181-8588

[5]TIS, 8-17-1 Nishi-shinjuku, Shinjuku-ku, Tokyo, 160-0023

*E-mail: morihana@nhao.jp

Received ; Accepted

Abstract

The Galactic Ridge X-ray Emission (GRXE) is apparently extended X-ray emission along the Galactic Plane. The X-ray spectrum is characterized by hard continuum with a strong Fe K emission feature in the 6–7 keV band. A substantial fraction ($\sim$80%) of the GRXE in the Fe band was resolved into point sources by deep Chandra imaging observations, thus GRXE is mostly composed of dim Galactic X-ray point sources at least in this energy band. To investigate the populations of these dim X-ray point sources, we carried out near-infrared (NIR) follow-up spectroscopic observations in two deep Chandra fields located in the Galactic plane at (l,b)=(0.1°, –1.4°) and (28.5°, 0.0°) using NTT/SofI and Subaru/MOIRCS. We obtained well-exposed NIR spectra from 65 objects and found that there are three main classes of Galactic sources based on the X-ray color and NIR spectral features: those having (A) hard

X-ray spectra and NIR emission features such as H I (Brγ), He I, and He II (2 objects), (B) soft X-ray spectra and NIR absorption features such as H I, Na I, Ca I, and CO (46 objects), and (C) hard X-ray spectra and NIR absorption features such as H I, Na I, Ca I and CO (17 objects). From these features, we argue that class A sources are cataclysmic variables (CVs), and class B sources are late-type stars with enhanced coronal activity, which is in agreement with current knowledge. Class C sources possibly belong to a new group of objects, which has been poorly studied so far. We argue that the candidate sources for class C are the binary systems hosting white dwarfs and late-type companions with very low accretion rates. It is likely that this newly recognized class of the sources contribute to a non-negligible fraction of the GRXE, especially in the Fe K band.

Key words: Galaxy: stellar content — X-rays: stars — stars: cataclysmic variables — stars: late-type — X-rays: diffuse background

1 Introduction

Since the dawn of the X-ray astronomy, apparently diffuse emission of low surface brightness has been known to exist along the Galactic Plane (GP; $|l| <45^\circ$, $|b| <1^\circ$)), which is referred to as the Galactic Ridge X-ray Emission (GRXE; e.g., Worrall et al. 1982; Warwick et al. 1985; Koyama et al. 1986). The X-ray spectrum is characterized by hard continuum with strong Fe K emission lines in the hard (2–8 keV) X-ray band (e.g., Koyama et al. 1986). The origin of the GRXE has been a mystery for a long time. A long-standing debate was whether it is a truly diffuse plasma (Ebisawa et al. 2001; Ebisawa et al. 2005) or the sum of dim unresolved X-ray point sources (Revnivtsev et al. 2006). Revnivtsev et al. (2009) claimed that most of the GRXE was resolved into dim X-ray point sources down to $\sim 10^{-16} \mathrm{ergs\ cm^{-2}\ s^{-1}}$ in the hard band using the deepest observation ($\sim$900 ks) made with the Chandra X-ray Observatory (Weisskopf et al. 2002) at a slightly off-plane region of (l,b)=(0.1°, –1.4°) in the Galactic bulge (Chandra bulge field; hereafter, CBF), which also known as the Limiting Window in the studies of van den Berg et al. (2009) and Hong (2012).

If the GRXE is composed of numerous dim X-ray point sources in the hard band, new questions arise : *What are the populations of these X-ray point sources? Which class of sources contribute to the Fe K emission lines?* There are several candidates for such sources. Revnivtsev et al. (2011) claimed that the majority of faint sources are X-ray active stars based on the luminosity function, while Hong (2012) argued that hard X-ray component of the GRXE above 3 keV is dominated by

sources such as magnetic cataclysmic variables (mCVs). However, it is difficult to constrain the nature of these point sources from X-ray data alone, because most of these sources are detected only with a limited number of X-ray photons even with the deepest observations. Follow-up spectroscopic studies in longer wavelengths are keys to elucidate the nature of individual X-ray sources.

In the optical band, several spectroscopic observations were carried out (Motch et al. 2010; van den Berg et al. 2012; Servillat et al. 2012; Nebot Gómez-Morán et al. 2013; van den Berg et al. 2006). They revealed that some X-ray sources are mCVs and late-type active stars, which was indeed speculated from optical and near-infrared (NIR) imaging studies of their work and other preceding work (Muno et al. 2004; Muno et al. 2009; van den Berg et al. 2009; Ebisawa et al. 2005). They also pointed out a small contribution from other classes of source, such as young stellar objects, Wolf-Rayet stars, γCas analogues, and symbiotic binaries.

Most of the X-ray sources studied in these optical studies are biased toward bright, or close, X-ray sources. This is because (i) the two XMM-Newton studies (Motch et al. 2010; Nebot Gómez-Morán et al. 2013) are based on wide and shallow surveys, which is $\sim$1 order magnitude shallower than the Chandra deep Galactic plane survey such as Ebisawa et al. (2005) and Grindlay et al. (2005), and (ii) the majority of the discrete X-ray sources comprising the GRXE are too attenuated by interstellar extinction to allow optical identification. Motch et al. (2010) estimated that only CVs within a 2 kpc distance are accessible within their optical survey limit.

To proceed further, we embarked on NIR spectroscopic follow-up studies based on the deepest Chandra data. $K_{\rm s}$-band extinction is about 10 times lower than V-band extinction, allowing access to the sources behind a large column of extinction. Here, we present the results of NIR follow-up study of dim X-ray sources constituting the GRXE. The outline of this paper is as follows. In §2, we present the data set and reduction. In §3, we show NIR spectra and classify sources based on the NIR spectra and X-ray colors. In §4, we discuss the nature of these classes and their contributions to the GRXE. Finally, we summarize our results in §5.

2 Observations

2.1 Data Sets

We first summarize the data sets in table 1. We use two GP fields that were studied with deep Chandra exposures: the CBF and the Ebisawa field at (l, b)=(28.5°, 0.0°) by Ebisawa et al. (2001). These two fields were studied in the NIR imaging surveys using the Simultaneous Infrared Imager for Unbiased Survey (SIRIUS; Nagashima et al. 1999, Nagayama et al. 2003) on the Infrared Survey Facility (IRSF) in the South African Astronomical Observatory and the Son of ISAAC (SofI: Moorwood et al.

1998) on the New Technology Telescope (NTT; Tarenghi & Wilson 1989) in the European Southern Observatory by Morihana (2012) and Ebisawa et al. (2005), respectively. In total, 222 out of 2002 (CBF) and 142 out of 274 (Ebisawa field) X-ray sources were identified with NIR sources in these studies.

Table 1. Data sets

Observations		CBF	Ebisawa field
	Telescope/Instrument	Chandra/ACIS-I	Chandra/ACIS-I
	Reference	Morihana et al. (2013)	Ebisawa et al. (2005)
NIR imaging	Number of sources†	222	142
	Telescope/Instrument	IRSF/SIRIUS	NTT/SofI
	Reference	Morihana (2012)	Ebisawa et al. (2005)
NIR spectroscopy	Number of sources‡	23	42
	Telescope/Instrument	Subaru/MOIRCS	NTT/SofI + Subaru/MOIRCS
	Reference	(this study)	(this study)

*The number of detected X-ray point sources.

†The number of X-ray point sources identified in the NIR imaging studies.

‡The number of NIR-identified X-ray point sources, for which well-exposed NIR spectra were obtained in this study.

We selected our NIR spectroscopy targets among these NIR-identified sources based on their X-ray spectral hardness, variability, and brightness. We used the NTT (§ 2.2.1) and the Subaru Telescope (§ 2.2.2) for observations. As our interest is to study origin of the sources contributing to the hard-band emission of GRXE, the selected targets are preferentially hard X-ray sources. Also, we selected sources with $K_{\rm s}$-band magnitude brighter than 14 mag for a reasonable telescope time. Among such sources, the false positive rate (a wrong counterpart pairs by chance) is estimated to be $\sim$3% (CBF) and $\sim$1% (Ebisawa field) by the product of the surface number density of NIR sources with $m_{K_{\rm s}} < 14$ mag and the maximum search circle. This is reasonably low to discuss statistical properties of subgroups, but the identification of individual sources is subject to contamination by false positives.

2.2 Observations & Data Reduction

2.2.1 NTT/SofI

We conducted a pilot observation of X-ray sources in the Ebisawa field using the SofI mounted at the Nasmyth focus of the NTT, which is located at the La Silla Observatory, Chile. The NTT is a 3.6 m Ritchey-Chrétien telescope on an altazimuth mount. The SofI is equipped with a 1024×1024 pixel

HgCdTe infrared array, and we used its long-slit spectroscopy mode with a medium-resolution grism ($R \sim 2200$) in the K_s band (2.0–2.3 μm) at a dispersion scale of $\sim$4.62 Å pixel^{-1}.

Table 2. NTT observation log

Ref.*	Coordinate (J2000.0)		SW†	$t_{\rm exp}$§	Airmass	Seeing‡
ID	R. A.	Decl.	(arcsec)	(min)		($''$)
SoE3	18:42:58.3	−03:53:27	1.0	20	1.14–1.19	1.1
SoE4	18:43:00.4	−03:53:49	1.0	20	1.11–1.11	1.3
SoE29	18:43:17.5	−03:56:00	1.0	4	1.11–1.12	1.0
SoE70	18:43:28.4	−04:07:33	1.0	2	1.68–1.76	1.2
SoE79	18:43:29.7	−03:50:15	1.0	20	1.12–1.16	1.8
SoE86	18:43:30.8	−04:01:03	1.0	2	1.91–2.01	1.1
SoE100	18:43:32.6	−04:04:19	1.0	4	1.38–1.45	0.9
SoE104	18:43:33.5	−04:03:54	2.0	2	1.54–1.60	1.2
SoE105	18:43:33.9	−03:52:53	1.0	36	1.16–1.28	1.9
SoE135	18:43:39.2	−03:52:53	1.0	2	2.06–2.17	1.2
SoE221	18:43:59.7	−03:55:18	1.0	2	1.78–1.87	1.1
SoE233	18:44:03.9	−04:02:58	1.0	36	1.16–1.29	1.1
SoE244	18:44:11.0	−04:05:17	1.0	24	1.10–1.13	1.4
SoE255	18:44:18.6	−04:06:03	1.0	20	1.11–1.13	1.8
SoE272	18:44:28.8	−04:01:03	2.0	16	1.62–1.92	1.8

*The reference source numbers follow Ebisawa et al. (2005).

† Slit width.

§ Total exposure time.

‡ Average seeing of all images in each slit.

We carried out the observation on 2005 July 18 and 19 for 16 selected X-ray sources, and well-exposed spectra were obtained from 15 of them (figure 1, table 2). Standard stars were also observed for the telluric correction, and the Xe-Ne lamp spectra were obtained for the wavelength calibration. Each spectrum was integrated for 30 or 60 s using a 1.″0 or 2.″0 slit width depending on their brightness. A set of spectra was composed of four spectra at two dithered positions (A and B) that are 60″ apart along the slit. From one to nine sets were obtained, resulting in a total net exposure time of 2 to 36 minutes. The seeing was 0.″9 to 1.″9 on the first night and 1.″0 to 1.″2 on the second night.

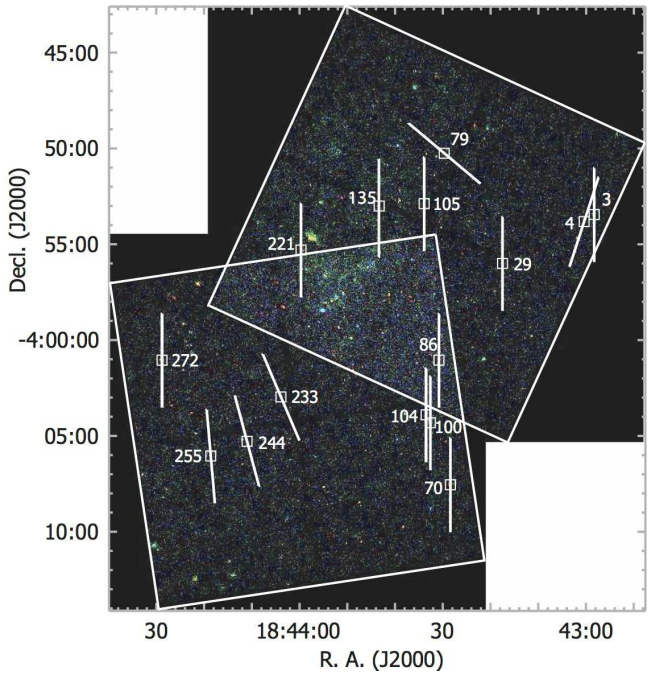

Fig. 1. Positions of the long slits for the SofI spectroscopy in the Ebisawa field. The background is the Chandra pseudo-color X-ray image and the boxes show the source location (see Table 2) used for the NIR spectroscopy with the sources numbers given in Ebisawa et al. (2005).

The SofI data were reduced using the standard procedures with the IRAF software package[1]. The frames were flat-fielded using dome flats and cleaned removing bad pixels and cosmic-ray events. Frames taken at the A and B positions were subtracted from each other to remove the dark current and sky emission. The frames were then combined, and the source spectra were extracted, registered for the wavelengths using the comparison lamp spectra fitted by a third-order polynomial. The calibration uncertainty is $\sim$0.32 Å. We then corrected for telluric features by dividing the A0 V standard star spectra, in which the Brγ feature is removed by a local Voigt profile fitting and the continuum is flattened by a 9790 K blackbody emission.

2.2.2 Subaru/MOIRCS

In order to increase the number of samples and to extend the samples to the fainter end, we further conducted multi-object NIR spectroscopy of X-ray sources both in the Ebisawa field and the CBF. We used the Multi-Object Infra-Red Camera and Spectrograph (MOIRCS; Ichikawa et al. 2006) at the Cassegrain focus of the 8.2 m Subaru Telescope in the Mauna Kea Observatory. MOIRCS is equipped with two adjacent HAWAII-2 arrays of 2048$\times$2048 pixels. The instrument is capable of obtaining multiple spectra simultaneously using a mask with multiple slits designed specifically for each field. We used the R $\sim$1300 grism in the $K_{\rm s}$-band (2.0–2.3 μm) with a dispersion scale of

[1] http://iraf.noao.edu/

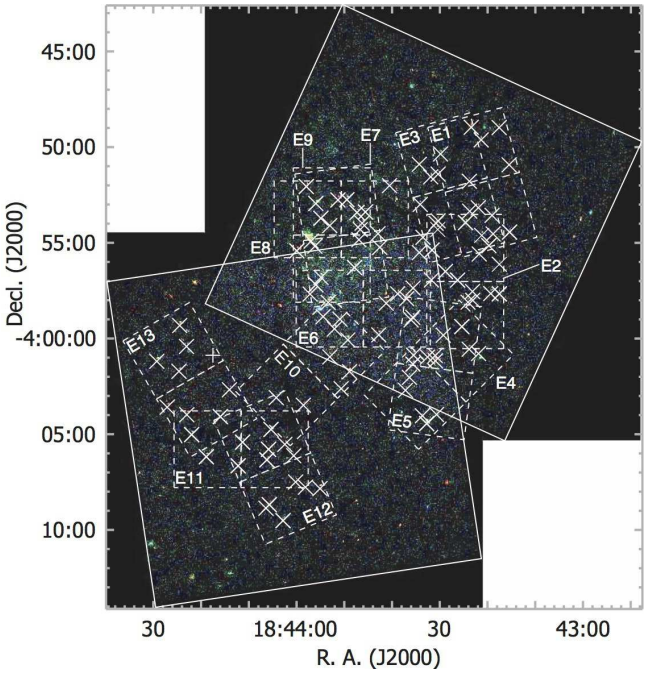

Fig. 2. Positions of the masks for the MOIRCS spectroscopy in the Ebisawa field. White dashed boxes show masks correspond to the Mask ID in table 3. White crosses indicate the source positions for which NIR spectra were obtained.

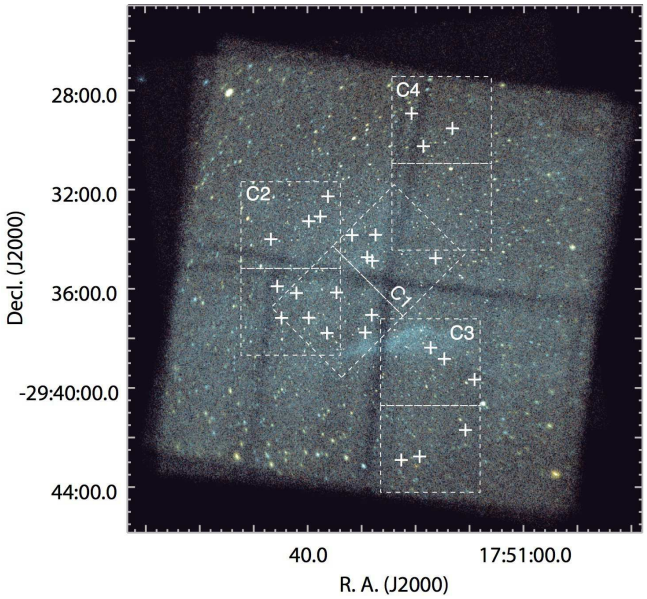

Fig. 3. Positions of the masks for the MOIRCS spectroscopy in the CBF. The symbols are the same as in figure 2.

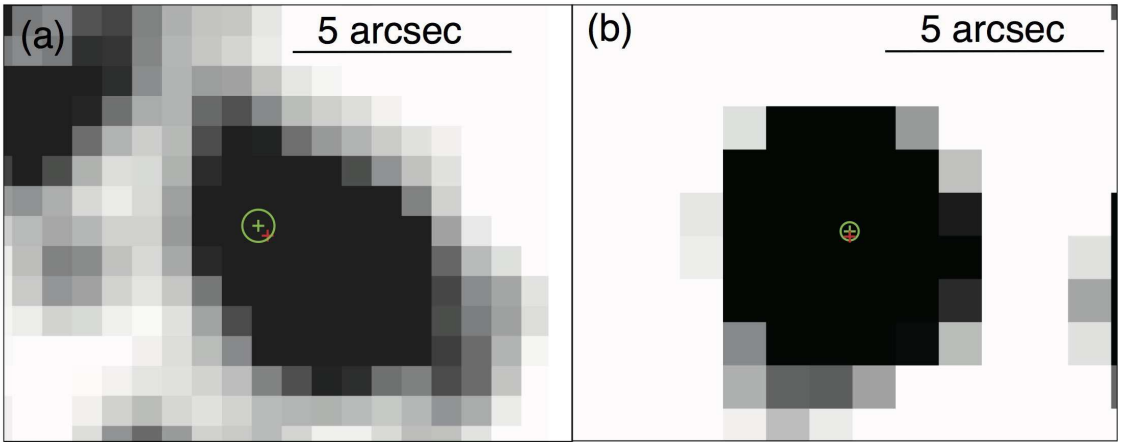

Fig. 4. Close-up view of the K_s-band image around two class A sources (a) source number 79 and (b) 100. The X-ray source position and its uncertainty are shown with a green cross and circle, while the position of its NIR counterpart is shown with a red cross.

$\sim$3.88 Å pixel^{-1}.

The observations were performed on 2007 June 07–10, 2008 June 27–28 (the Ebisawa field; figure 2) and on 2011 June 23–24 (the CBF; figure 3). We designed masks so that we can cover as many sources as possible. Each mask has 6–15 slits (table 3), and 2–3 masks were used each night. The A–B–B–A dithering pattern was repeated several times for each mask. We used the OH emission lines in the sky spectra for the wavelength calibration in both fields. This resulted in saving some telescope time, but a degraded calibration accuracy in the longer wavelengths in the K_s-band where the OH emission features are sparse. In each night, we took standard stars several times using one of the slits of a mask, so that one of them has a similar airmass with the target objects.

The MOIRCS data were also reduced using the standard procedure in the same manner as the SofI data. In addition, we applied the distortion correction according to the recipe provided by the instrument team[2]. We generated both A–B and A+B frames respectively for the source and sky spectra; the latter were used for wavelength calibration, resulting in a calibration uncertainty of $\sim$0.28 Å. We stacked all the frames taken with the same chip with the same mask, and extracted spectra, and corrected for the tellulic features using the standard star spectra.

3 Results

3.1 NIR Spectra

With the NTT/SofI and Subaru/MOIRCS observations combined, we obtained well-exposed spectra from a total of 23 and 44 different objects in the CBF and the Ebisawa field, respectively. Properties

[2] See http://www.naoj.org/staff/ichi/MCSRED/mcsred.html for detail.

Table 3. Subaru observation log

Mask ID*	Coordinate (J2000.0)		$t_{\rm exp}$†	Num. of slits	Airmass	Seeing‡
	R. A.	Decl.	(min)			($''$)
C1	17:51:29	−29:35:43	180	15	1.55–1.97	0.8
C2	17:51:43	−29:34:47	165	15	1.63–2.02	1.3
C3	17:51:17	−29:40:60	140	13	1.55–1.83	0.7
C4	17:51:16	−29:31:02	160	10	1.53–1.85	0.9
E1	18:42:52	−03:53:29	12	7	1.00–1.62	0.3
E2	18:42:53	−03:52:01	24	7	1.09–1.29	0.3
E3	18:43:24	−04:02:01	32	14	1.47–1.73	0.5
E4	18:43:50	−03:53:40	24	14	1.23–1.88	0.5
E5	18:43:30	−04:01:26	18	9	1.09–1.32	0.3
E6	18:43:45	−03:58:20	24	11	1.22–1.52	0.7
E7	18:43:50	−03:53:39	30	12	1.09–1.14	0.3
E8	18:43:40	−04:01:48	45	7	1.21–1.60	0.3
E9	18:43:25	−03:56:55	40	11	1.09–1.12	0.4
E10	18:43:57	−04:01:37	40	6	1.18–1.49	0.4
E11	18:43:21	−03:51:41	45	9	1.21–1.68	0.4
E12	18:43:51	−03:54:20	45	9	1.09–1.12	0.5
E13	18:44:05	−04:06:26	40	11	1.20–1.59	0.9

* "C" shows the CBF and "E" shows the Ebisawa field.

† Exposure time.

‡ Average seeing of all images in each mask.

of all the spectra are summarized in table 4 and table 5. The spectra are shown in figures 5 and 6. The continuum was fitted with a polynomial and was subtracted, and then, normalized in an arbitrary unit for the display.

We notice that the sources can be divided into two simply based on whether the features are dominated by absorption or emission: (i) Sources with absorption lines such as H I, Na I (2.21 μm), Ca I (2.26 μm), and CO bandhead features (2.29, 2.32, 2.35, 2.38 μm). (ii) Sources with emission lines such as H I (Brγ: 2.16 μm), He I (2.11 μm), and He II (2.19 μm),

For (i) sources, we estimated the spectral type by comparing the NIR spectral atlas of cool stars (Ali et al. 1995; Rayner et al. 2009) assuming that they are dwarfs. We estimated a rough spectral type for each NIR spectrum. F- and G-type stars exhibit Brγ absorption line (H I). G-type

stars also show metallic features such as Na I, Ca I. K- and M-type stars have molecular features of CO and with little metallic features. The CO absorption features are dominant in the M-type stars more than in the K-type stars. The proposed spectral types are shown in table 4 and 5. For (ii), we labelled them as "em" in table 4. The difference in the luminosity class (dwarf or giants) cannot be distinguished with the spectral resolution in the presented study, but it does not affect the rough spectral typing described above (Rayner et al. 2009).

3.2 X-ray Spectra

Since most X-ray sources are too dim to make individual X-ray spectrum, we use hardness ratio to characterize X-ray spectra. We define the spectral hardness ratio as HR = (H-S)/(H+S), where H and S are the normalized count rate in the hard (2–8 keV) and soft (0.5–2 keV) energy band. We calculated the HR for each source in the both fields and show them in tables 4 and 5. Based on X-ray hardness and NIR spectral features, we can classify sources into three: those with (A) hard X-ray spectra (HR$\geq$0.11) and NIR emission features such as H I (Brγ), He I, and He II (2 objects), (B) soft X-ray spectra (HR$<$0.11) and NIR absorption features such as H I, Na I, Ca I and CO bandheads (46 objects), and (C) hard X-ray spectra (HR$\geq$0.11) and NIR absorption features such as H I, Na I, Ca I and CO bandheads (17 objects).

To characterize the X-ray spectral features further, we made a composite X-ray spectrum in the 0.5–8.0 keV of each class (figure 7). Note that the composite spectrum is the sum (not the average) of the spectra of individual sources. Each X-ray spectra in 0.5- 8 keV were binned so that each bin includes more than 20 counts in order to use the χ^2 statistics. For the spectral models, we first used a one-temperature optically-thin thermal plasma model (APEC, Smith et al. 2001) convolved with an interstellar absorption model (Wilms et al. 2000) with the interstellar abundance by Anders & Grevesse (1989). This thermal model includes the Fe K line, of which strength is characterized with metal abundance parameter relative to solar abundance (Z) (table 6). Though the fits are barely acceptable, they give a general idea of the spectral shape, such that the composite spectrum of class A source seems to be best described by a single high temperature component, while class B and C seem to require an additional component. We then added another one-temperature plasma model. From the fitting, it is found that the X-ray spectra of class A and C are dominated by the higher temperature component, while that of the class B is by the lower temperature component.

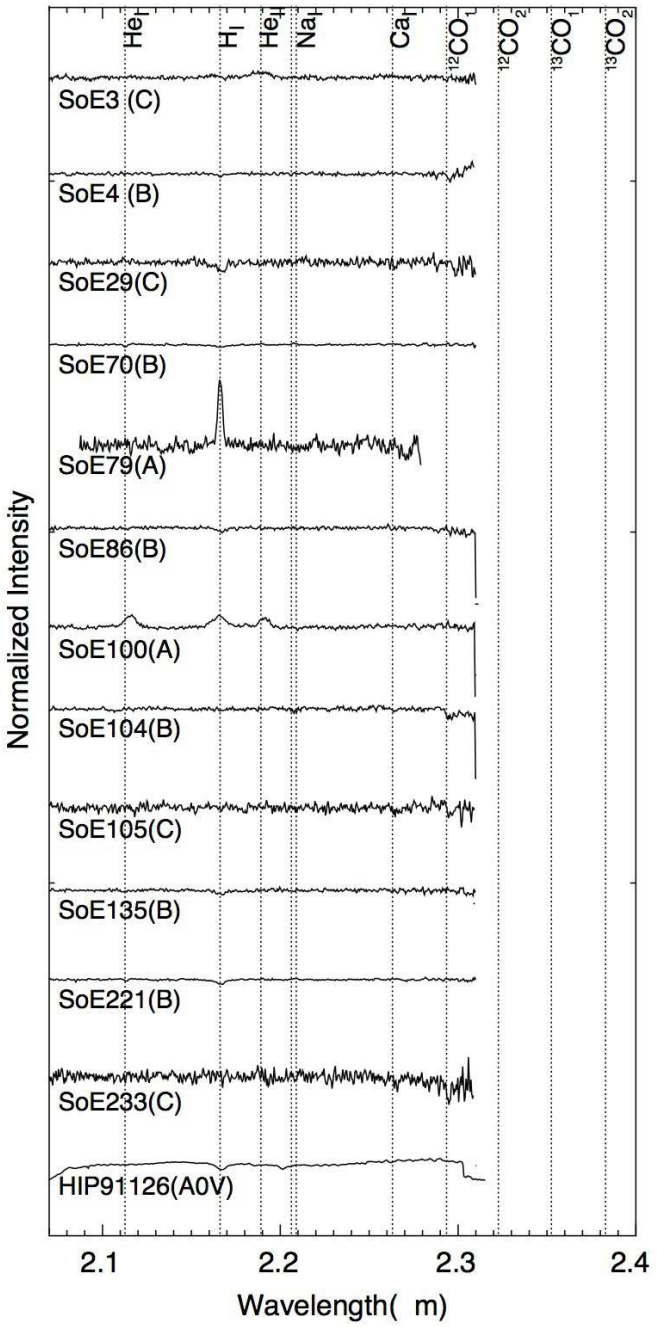

Fig. 5. Normalized K_s-band spectra of sources in the Ebisawa field using NTT/SofI and Subaru/MOIRCS. Source numbers follow tables 4 and 5. SoE indicates that the spectra were obtained in the Ebisawa field with NTT/SofI and SuE indicates by Subaru/MOIRCS. The proposed class (A, B, and C; see § 3.2) is also given for each spectrum. At the top, some spectroscopic features are labelled. Two ^{12}CO and ^{13}CO features are distinguished by suffix 1 and 2. At the bottom, standard star (A0V) spectra are shown, which are not corrected for telluric features to highlight these features with the ⊕ marks.

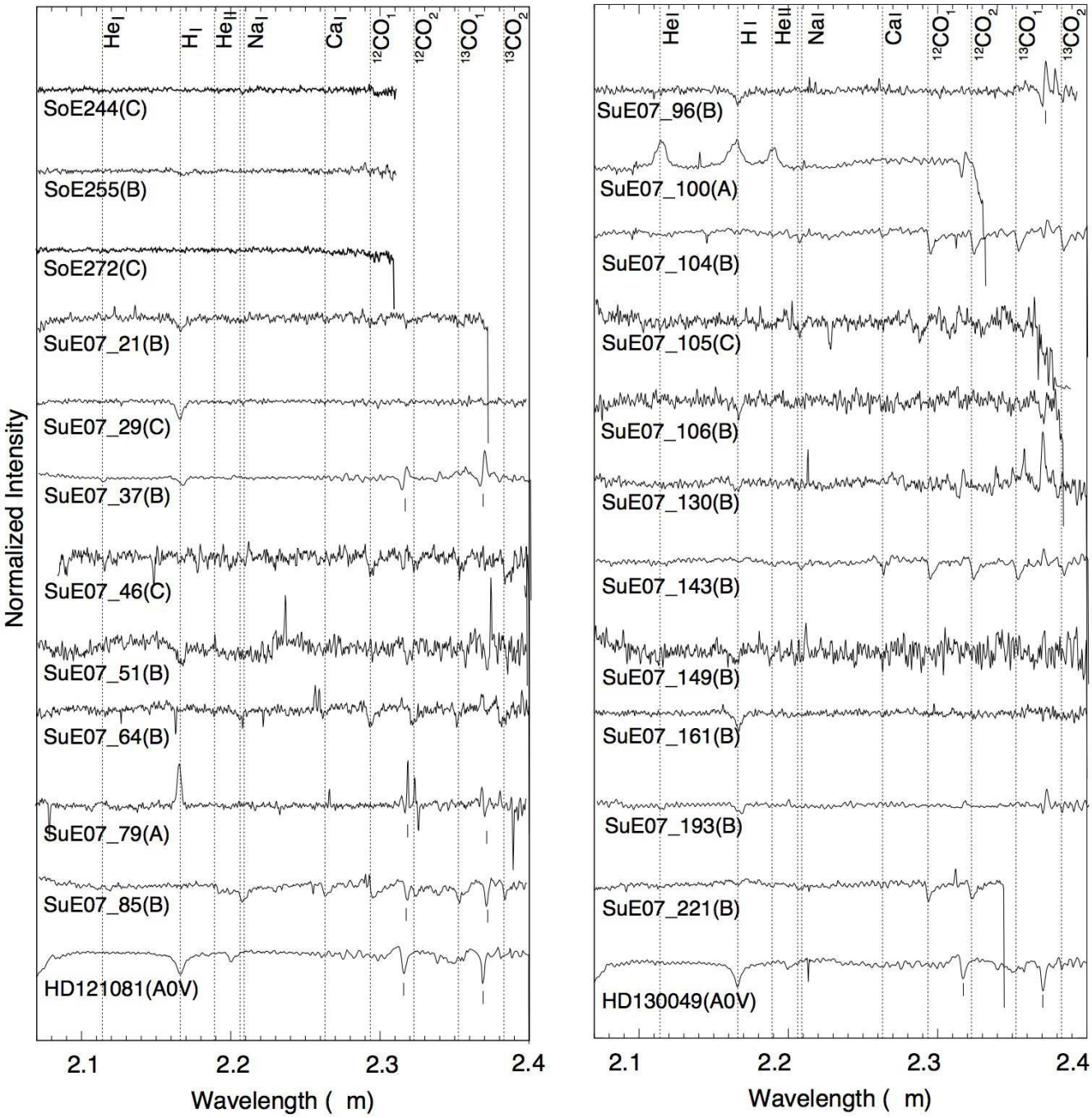

Fig. 5. (Continued).

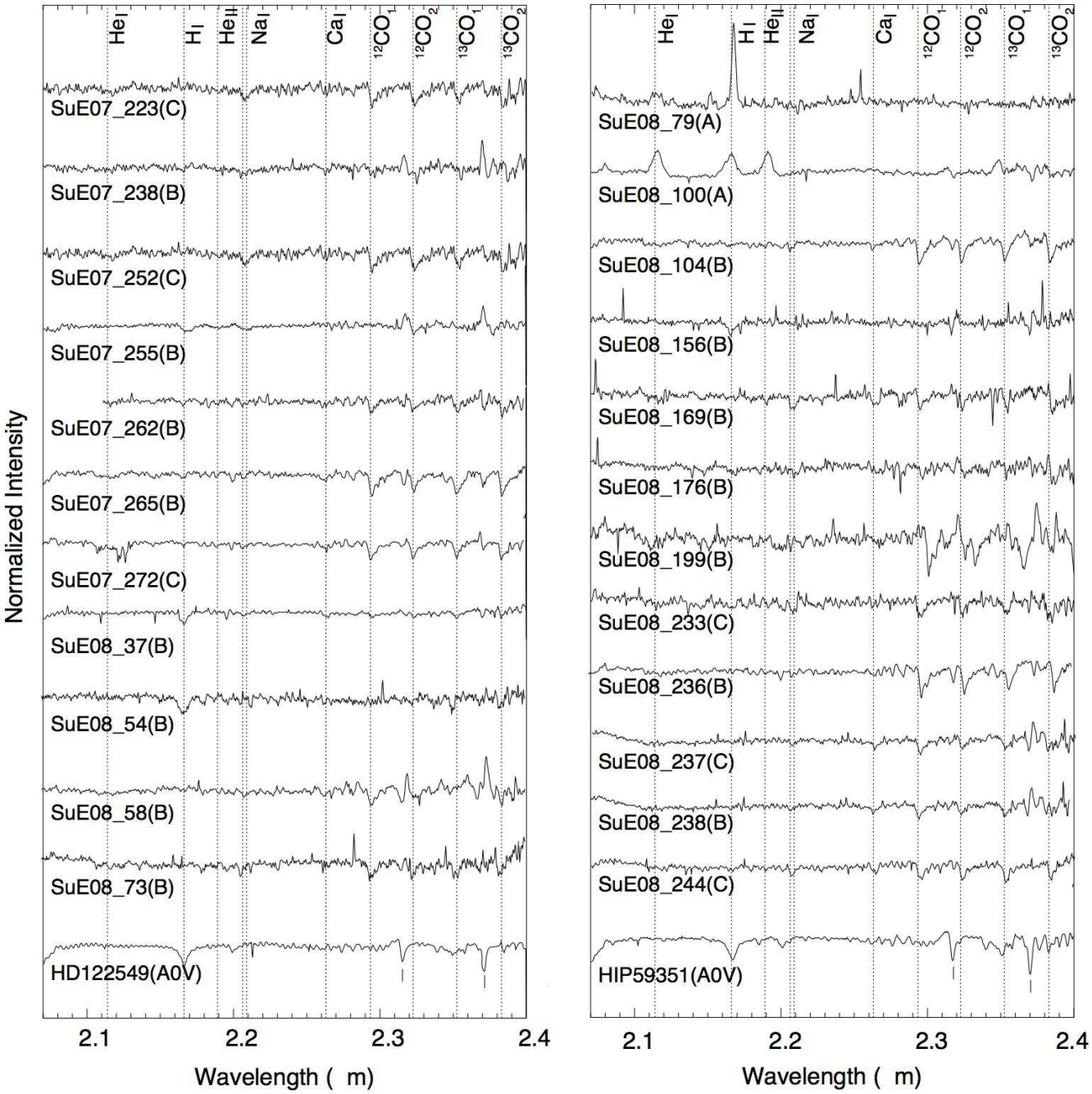

Fig. 5. (Continued.)

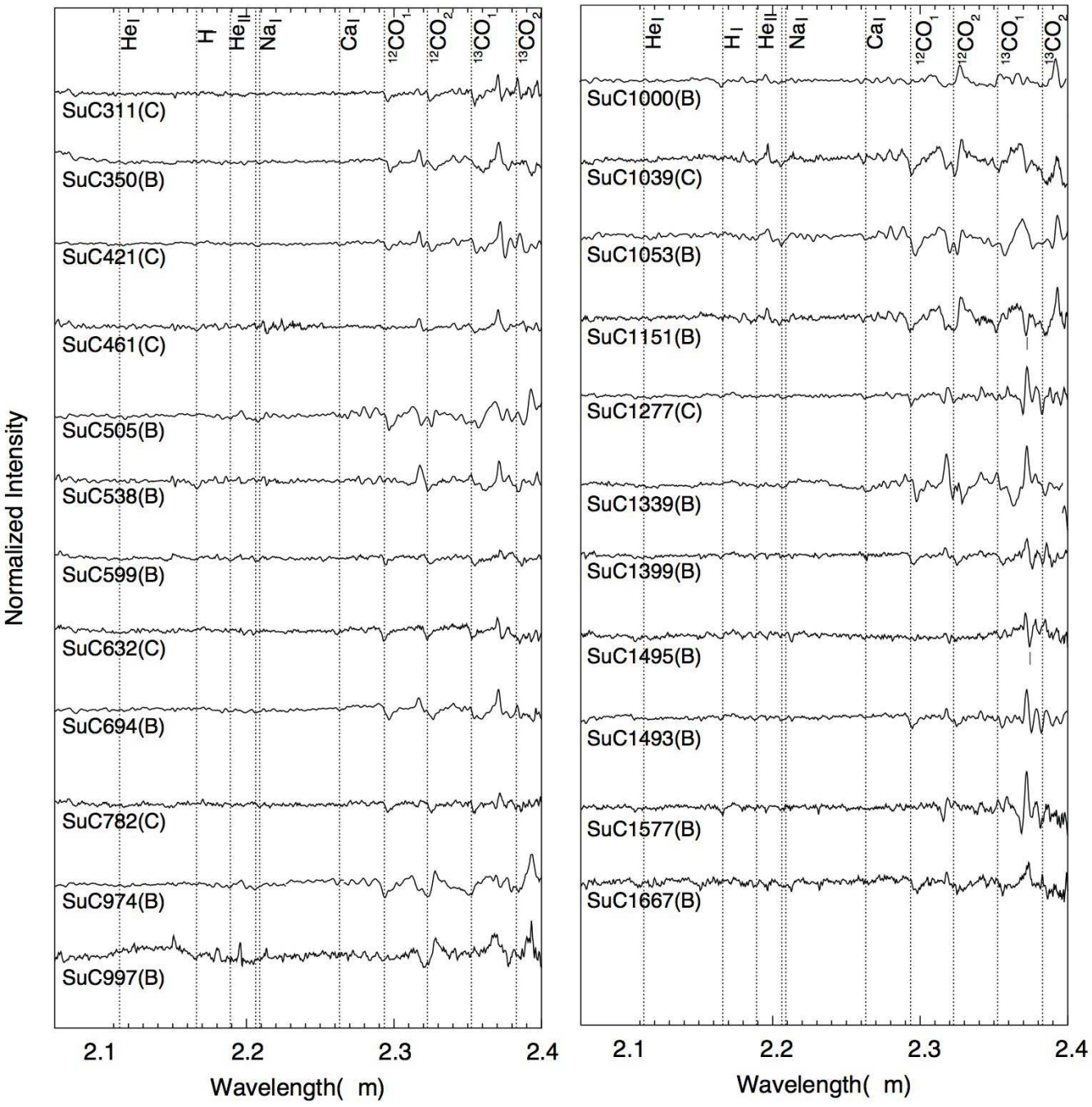

Fig. 6. Normalized K_s-band spectra of sources in the CBF using Subaru/MOIRCS. Source numbers follow table 5. Other symbols are the same with figure 5.

Table 4. NIR spectra obtained in the Ebisawa field

Ref.∗	R. A. Decl.	HR	m_{K_s}	H–K_s†	log	Obs‡	Features§								Proposed‖	Class#
ID	(J2000.0)		(mag)	(mag)	(F_X/F_{Ks})		He I	H I	He II	Na I	Ca I	$^{12}CO_1$	$^{12}CO_2$	$^{13}CO_1$	$^{13}CO_2$	type	
3	18:42:58.3−03:53:27	0.86	12.5	2.20	−1.65	SoE		+								late G	C
4	18:43:00.4−03:53:49	−0.03	12.1	1.60	−2.24	SoE						+				early K	B
21	18:43:13.8−03:57:07	−0.24	12.7	0.34	−3.14	SuE_07		+				+				early K	B
29	18:43:17.5−03:56:00	0.29	12.0	0.14	−2.74	SoE		+								early K	C
						SuE_07		+								early K	C
37	18:43:19.0−03:53:27	−0.54	12.8	0.18	−3.69	SuE_07		+								late K	B
						SuE_08		+				+	+			late K	B
46	18:43:21.1−03:54:30	0.60	14.6	–	−1.60	SuE_07		+								early K	C
51	18:43:21.8−03:53:03	−0.40	13.3	0.23	−2.44	SuE_07		+								early K	B
54	18:43:23.0−03:57:53	−0.44	13.3	0.23	−2.93	SuE_08		+								early K	B
58	18:43:23.6−03:53:14	0.09	14.4	0.19	−2.27	SuE_08						+				late K–early M	B
64	18:43:24.5−03:53:50	−0.31	12.2	0.43	−2.21	SuE_07						+	+	+	+	late K–early M	B
70	18:43:28.4−04:07:33	−0.72	8.5	0.15	−3.94	SoE	+	+								late G	B
73	18:43:28.9−03:57:33	−0.56	13.2	0.34	−2.47	SuE_08		+				+	+	+		late K–early M	B
79	18:43:29.7−03:50:15	0.99	12.9	Non	−2.07	SoE		–								em	A
						SuE_07		–								em	A
						SuE_08		–								em	A
85	18:43:30.6−03:53:52	−1.00	11.0	0.26	−4.13	SuE_07		+		+	+	+				late K	B
86	18:43:30.8−04:01:03	−0.74	9.3	0.13	−3.97	SoE		+								late G	B
96	18:43:31.8−03:57:17	−0.33	13.9	1.70	−2.72	SuE_07		+								early K	B
100	18:43:32.6−04:04:19	0.74	11.1	1.41	−1.97	SoE	–	–	–							em	A
						SuE_07	–	–	–							em	A
						SuE_08	–	–	–							em	A
104	18:43:33.5−04:03:54	−0.29	10.4	0.36	−3.44	SoE						+				early M	B
						SuE_07						+	+	+	+	early M	B
						SuE_08						+	+	+	+	early M	B
105	18:43:33.9−03:52:53	0.70	13.1	1.80	−2.42	SoE		+								?	C
						SuE_07				+						late K–early M	C
106	18:43:34.1−03:55:24	−0.67	14.1	0.37	−2.90	SuE_07		+								early K	B

Table 4. (Continued)

Ref.*	R. A.	Decl.	HR	m_{K_s}	H–K_s†	log	Obs‡	Features§								Proposed‖	Class#
ID	(J2000.0)			(mag)	(mag)	(F_X/F_{Ks})		He I	H I	He II	Na I	Ca I	$^{12}CO_1$	$^{12}CO_2$	$^{13}CO_1$	$^{13}CO_2$	type	
130	18:43:49.5	−03:52:33	−0.60	12.6	0.30	−3.24	SuE_07		+								late G–early K	B
135	18:43:39.2	−03:52:53	−0.79	9.9	0.36	−4.05	SoE		+								early K	B
143	18:43:41.0	−03:58:02	−0.50	10.7	0.45	−3.70	SuE_07		+		+	+	+	+	+	+	late K–early M	B
149	18:43:42.6	−03:59:41	−0.13	14.5	0.19	−1.97	SuE_07		+								late G–early K	B
156	18:43:45.4	−03:53:17	−0.60	13.8	0.27	−2.26	SuE_08		+								late G–early K	B
161	18:43:46.4	−03:54:12	−0.83	13.4	0.17	−2.95	SuE_07		+								late G–early K	B
169	18:43:47.1	−03:53:18	−0.29	14.2	0.37	−1.88	SuE_08				+		+	+			late G- early K	B
176	18:43:48.7	−04:01:36	−0.56	13.4	0.24	−2.36	SuE_08		+		+	+					K	B
193	18:43:53.1	−03:57:60	−0.16	12.7	0.22	−2.66	SuE_07		+								late G–early K	B
199	18:43:54.8	−04:07:42	0.06	13.3	0.25	−2.36	SuE_08		+				+	+	+	+	late K–M	B
221	18:43:59.7	−03:55:18	−0.53	8.8	0.17	−4.20	SoE		+								early K	B
							SuE_07		+				+	+			early K–late K	B
223	18:44:00.3	−04:05:59	0.50	11.9	0.46	−2.91	SuE_07		+		+		+	+	+	+	late K–early M	C
233	18:44:03.9	−04:02:58	0.25	13.4	0.82	−1.46	SoE						+				lateK–early M	C
							SuE_07				+		+	+	+	+	late K–early M	C
							SuE_08						+	+	+	+	late K–early M	C
236	18:44:05.4	−04:08:32	−0.73	14.1	0.24	−2.05	SuE_08						+	+	+	+	late K -early M	B
237	18:44:05.6	−04:05:39	0.14	14.9	0.41	−1.81	SuE_08		+		+	+	+	+	+		late K–early M	C
238	18:44:05.9	−04:06:12	0.01	13.1	0.26	−2.12	SuE_07		+		+	+	+	+	+		late K–early M	B
							SuE_08		+		+	+	+	+	+	+	late K–early M	B
244	18:44:11.0	−04:05:17	0.48	12.7	0.84	−2.20	SoE				+						late K–early M	C
							SuE_08				+		+	+	+	+	late K–early M	C
252	18:44:15.6	−04:03:57	0.79	13.6	0.99	−1.98	SuE_07		+		+		+	+	+		late K–early M	C
							SuE_08						+	+	+	+	late K– M	C
255	18:44:18.6	−04:06:03	0.06	12.1	0.48	−2.60	SoE		+								K	B
							SuE_07		+		+						K	B
262	18:44:22.7	−04:00:17	0.10	12.5	0.87	−2.56	SuE_07						+	+	+		late M	B
265	18:44:24.2	−04:01:35	−0.09	13.8	0.87	−2.03	SuE_07						+	+	+	+	late M	B
272	18:44:28.8	−04:01:03	0.27	11.1	0.72	−2.37	SoE						+				late K–M	C
							SuE_07						+	+	+	+	late K–M	C

* Sequence ID in Ebisawa et al. (2005). † Non : no detection in H-band. ‡ SoE : NTT/SofI observation source, SuE_07: Subaru/MOIRCS observation source, SuE_08:Subaru/MOIRCS 2008 observation source. § + shows absorption features and – shows emission features. ‖ Proposed spectral types based on each spectral features. ? : difficult to determine spectral type with low S/N features. em : spectra with emission features such as H I, He I, and He II. # A, B, and C indicate the proposed class we defined in § 3.2.

Table 5. NIR Spectra obtained in the Chandra Bulge Field

Ref.*	R. A.	Decl.	HR	m_{K_s}	H–K_s†	log	Features‡								Proposed§	Class‖
ID	(J2000.0)			(mag)	(mag)	(F_X/F_{Ks})	He I	H I	He II	Na I	Ca I	$^{12}CO_1$	$^{12}CO_2$	$^{13}CO_1$	$^{13}CO_2$	type	
311	17:51:09.2	−29:39:39	0.42	11.7	0.29	−3.34						+	+	+		late K	C
350	17:51:10.7	−29:41:40	−0.17	11.8	0.32	−3.22						+	+			early M	B
421	17:51:13.3	−29:29:31	0.41	13.9	0.67	−2.41		+		+	+	+	+	+		late K–early M	C
461	17:51:14.8	−29:38:50	0.38	13.0	0.29	−2.84		+								early K	C
505	17:51:16.3	−29:34:46	0.10	14.0	0.28	−2.95				+						K	B
538	17:51:17.2	−29:38:23	−0.95	12.0	0.06	−4.13		+					+			K	B
599	17:51:18.6	−29:30:15	−0.26	11.1	0.37	−3.84						+	+	+		late K–early M	B
632	17:51:19.4	−29:42:46	0.91	13.3	0.41	−2.54						+	+	+		late K–early M	C
694	17:51:20.7	−29:28:56	−0.09	10.8	0.50	−3.95						+	+	+		late K–M	B
782	17:51:22.6	−29:42:54	0.52	13.3	0.24	−2.16						+	+	+		late K–M	C
974	17:51:27.5	−29:33:51	−0.76	11.4	0.39	−3.82						+	+	+	+	M	B
997	17:51:46.5	−29:34:01	−0.97	13.5	Non	−3.35							+			M	B
1000	17:51:28.1	−29:37:03	−0.84	10.9	0.03	−4.31		+								early K	B
1039	17:51:29.1	−29:34:44	0.20	12.5	0.38	−3.46				+		+	+	+		late K	C
1053	17:51:29.4	−29:37:46	0.01	10.8	0.43	−4.57				+		+	+			M	B
1151	17:51:31.8	−29:33:51	−0.12	12.7	0.29	−3.46				+		+	+	+		M	B
1277	17:51:34.5	−29:36:09	0.24	13.8	0.14	−2.60				+		+				M	C
1339	17:51:36.4	−29:32:17	−0.05	13.1	0.47	−2.96				+		+	+			M	B
1399	17:51:37.7	−29:33:05	−0.78	11.5	0.24	−3.92				+		+	+	+		early M	B
1495	17:51:39.8	−29:37:10	−0.82	13.3	0.02	−3.06				+						?	B
1493	17:51:39.8	−29:33:18	−0.19	11.7	0.26	−3.96				+		+	+			early K	B
1577	17:51:42.1	−29:35:37	0.06	13.1	0.06	−3.63		+								early K	B
1667	17:51:44.8	−29:37:12	−0.15	13.0	0.32	−3.86						+	+	+		early M	B

* Sequence ID in Morihana et al. (2013). † Non : no detection in H-band. ‡ + shows absorption features and – shows emission features. § Proposed spectral types based on each spectral features. ? : difficult to determine spectral type. ‖ Class A, B, and C indicate proposed class we defined in § 3.2.

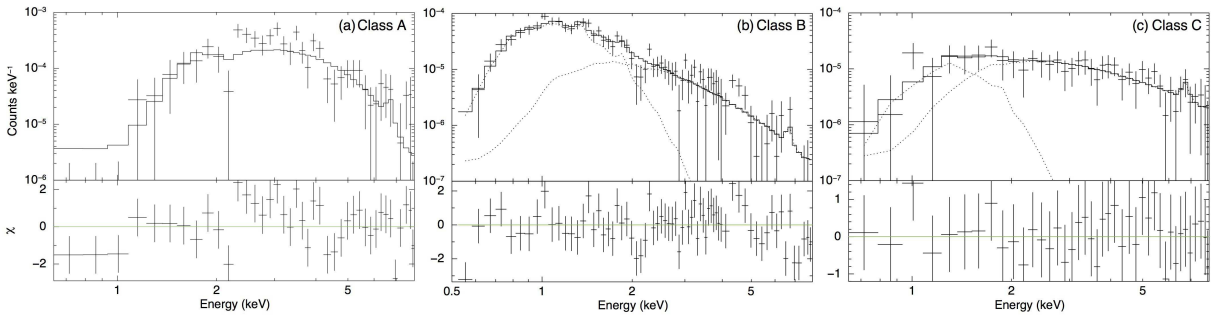

Fig. 7. Composite spectra and the best-fit models of the three classes. Grouped data (pluses) and the best-fit model convolved with the instrumental response (solid histograms) are shown in the upper panel, while the residuals to the fit are shown in the lower panel. The best-fit parameters are given in table 6.

Table 6. Best-fit parameters for global spectral fittings∗

Class	$N_{\rm H}$ ($\times 10^{22}$ cm^{-2})	$k_{\rm B}T_1$ (keV)	$k_{\rm B}T_2$ (keV)	Z†	χ^2/d.o.f
A	$3.66^{+0.74}_{-0.53}$	$3.63^{+1.35}_{-1.12}$	–	$0.21^{+0.78}_{-0.15}$	57.54/38
B	$1.38^{+0.19}_{-0.10}$	$0.27^{+0.08}_{-0.08}$	$2.04^{+0.74}_{-0.53}$	$0.15^{+0.32}_{-0.10}$	82.21/64
C	$2.32^{+0.87}_{-0.78}$	$0.21^{+0.20}_{-0.09}$	$5.37^{+1.95}_{-2.17}$	$0.24^{+0.49}_{-0.20}$	13.29/35

∗The best-fit value and a 1σ statistical uncertainty are given.

† Metal abundance relative to the solar value.

4 Discussion

4.1 Classification

We discuss the nature of the sources for the three classes defined in § 3.2. First, we argue that class A sources (ID 79 and 100 in Ebisawa field) are CVs for the following reasons : (i) They are hard X-ray sources with large HR values (HR of ID 79 and 100 are 0.71 and 0.11, respectively). (ii) A probable Fe K feature and a dominant high-temperature ($\sim$4 keV) plasma (table 6) are seen in the composite X-ray spectrum. (iii) They also exhibit NIR spectra with H I (Brγ), He I, and He II emission lines, which presumably arise from the accretion disk. All of these are the established observational characteristics of CVs (e.g., Ezuka & Ishida 1999, Baskill et al. 2005, Dhillon et al. 1997).

Second, we argue that class B sources are late-type stars with enhanced coronal X-ray activities (X-ray active stars) for the following reasons : (i) They show a soft X-ray spectrum (table 6), in which the low-temperature (0.3 keV) component is dominant. The low-temperature component is presumably from the stellar corona, and the high-temperature component is from flares. (ii) They exhibit NIR spectra with the absorption lines commonly seen from the cool stars such as H I, Na I, Ca I, and CO bandheads.

The presence of the class A and B populations is no surprise, which is perfectly compatible

with current understandings of the population of faint Galactic X-ray point sources as discussed in §1. Before starting the presented study, we had anticipated that most of our sources would be from these classes. Now, class C appeared as an unexpected new class, which has not been recognized so far. Rather surprisingly, only 2 of the 19 NIR spectra of hard X-ray sources are class A (CV) whereas a majority of them (17 of 19 sources) are class C.

We critically examine the possibility that the class C sources are not intrinsically hard X-ray sources but only apparently hard due to larger Galactic extinctions than class B sources that share the same NIR characteristics as class C sources. We investigated individual sources by plotting X-ray hardness (HR) versus infrared color, H–K_s (figure 8). As the extinction increases, the H–K_s and the HR values become larger along the extinction curve. The extinction curves are shown for some representative sources of CVs (for class A) and X-ray active stars (for class B). It is found that class C sources are not on the extinction curve of class B sources. Therefore, class C sources are likely to represent a new class distinctive from class A and B.

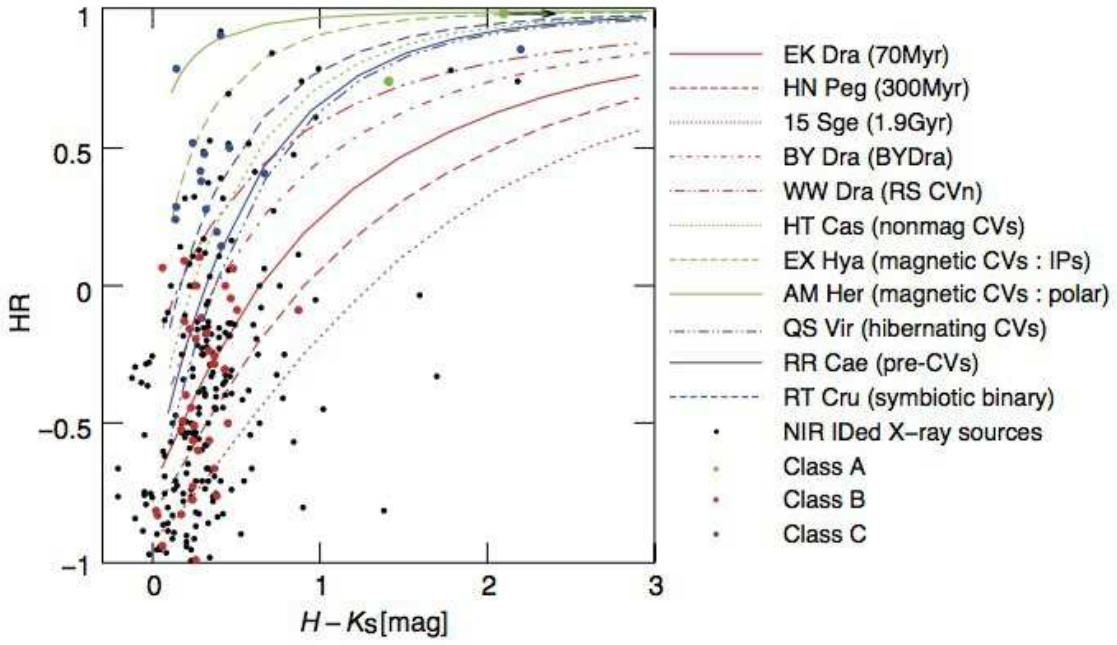

Fig. 8. Scatter plot of X-ray versus NIR colors (i.e., HR versus H–K_s) for all the X-ray sources identified in the NIR imaging studies (small dots). For a source with no H-band detection, a black arrow is shown. Those with NIR spectra are shown with large circles with different colors for different classes. The extinction curves are calculated for some representative sources by assuming an intrinsic NIR color (Cox 2000) and X-ray spectrum from the following work: (1) X-ray active single single stars with different ages (EK Dra: 70 Myr, HN Peg: 300 Myr, and 15 Sge: 1.9 Gyr; Güdel et al. 1999), (2) X-ray active binary stars (BY Dra; Dempsey et al. 1997, WW Dra ; Dempsey et al. 1993), (3) a non-magnetic CV (HT Cas ; Nucita et al. 2009), (4) an intermediate polar (EX Hya; Allan et al. 1998), (5) a polar (AM Her; Ishida et al. 1997), (6) hibernating CVs (QS Vir ; Matranga et al. 2012), (7) pre-cataclysmic variables (RR Cae ; Bilíková et al. 2010a), and (8) symbiotic bianries (RT Cru; Luna & Sokoloski 2007). We calculate the expected H–K_s using $N_{\rm H}$= $3.5\times10^{22}\times E\,(H–K_s)$ cm^{-2} (Nebot Gómez-Morán et al. 2013).

What are the new class C sources? We calculated the X-ray to NIR flux ratio (absorption not corrected) for all the sources in tables 4 and 5. We used the hard band for the X-ray and $K_{\rm s}$ band for the NIR flux to minimize the effect of interstellar attenuation. The median of the $F_{\rm X}/F_{\rm Ks}$ values are 9.4×10^{-3} (class A), 7.8×10^{-4} (class B), and 8.4×10^{-3} (class C), while the rms of the values are 1.3×10^{-3} (class A), 1.3×10^{-4} (class B), and 2.2×10^{-3} (class C).

We estimated $F_{\rm X}/F_{\rm Ks}$ of CVs using Baskill et al. (2005) and Ezuka & Ishida (1999), and found that their values are always larger than $F_{\rm X}/F_{\rm Ks}$=1.35×10^{-3}. We also investigated $F_{\rm X}/F_{\rm Ks}$ of X-ray active stars in Pandey & Singh (2008) and Pandey & Singh (2012). In contrast to CVs, only 2 of 10 sources have $F_{\rm X}/F_{\rm Ks}$ values greater than $\sim10^{-3}$ (the highest is 5.5×10^{-3}) and the rest have much smaller values of $F_{\rm X}/F_{\rm Ks}$ between 10^{-6} and 10^{-4}. Comparing these values with the average $F_{\rm X}/F_{\rm Ks}$ values of class A, B and C sources, the class A and B are most likely to be CVs and X-ray active stars, respectively. Most class C sources are presumably systems holding white dwarfs like CVs, but may include some extremely X-ray active stars.

As mentioned above, class C has the following characteristics as a group: (1) large $F_{\rm X}/F_{\rm Ks}$ values as those for CVs. (2) NIR spectra show no emission lines, but only absorption features of cool stars. (3) Hard X-ray spectra showing a possible Fe K feature (see figure 7). The fact (1) suggests degenerate system with low accretion rates. From (2), class C sources are probably not CVs, since CVs show emission lines such as H I (Brγ), He I, and He II (e.g., Dhillon & Marsh 1995; Dhillon et al. 1997). From (3), active stars and binaries, which show relatively soft X-ray energy spectra, are probably ruled out. Also, we consider that the majority of our class C sources are not HMXBs either, that are known not to be the dominant population of hard X-ray sources (e.g., Laycock et al. 2005).

Therefore, class C are likely to be other binary systems holding degenerate stars. Some binaries including white dwarfs, such as QS Vir and V471 Tau, are known to have similar properties to class C, namely, strong Fe K emission line in X-rays with low X-ray luminosities of $L_{\rm X}$ = 10^{28-29} erg s^{-1} (e.g., Matranga et al. 2012, Bilíková et al. 2010b) and the Na I, Ca I, and CO absorption lines in NIR (e.g., Howell et al. 2010).

In fact, there are several such populations to exhibit the characteristics of class C that are hibernating CVs, pre-Cataclysmic Variables (pre-CVs), and symbiotic binaries. Hibernating CVs are temporarily or marginally detached binary systems hosting a white dwarf and a dwarf star where no or little accretion takes place. Pre-CVs are detached binary systems hosting a white dwarf and a late-type star (mainly M -dwarf) with low level accretion, as opposed to the conventional CVs that are semi-detached systems with high level accretion. Since both populations have been poorly

studied, it is conceivable that there might be a lot of undiscovered hibernating CVs and pre-CVs in our Galaxy. Recently, the number of white dwarf binaries, including detached systems, has increased significantly by large surveys such as the Sloan Digital Sky Survey and follow-up observations being likely to continue to grow in future (Ritter & Kolb 2003 and its online updates at `http://wwwmpa.mpa-garching.mpg.de/RKcat/`). Alternatively, symbiotic binaries, which are interacting binaries consisting of a mass-losing red giant and a blue companion (mainly white dwarf), is another candidate population of the new class. Symbiotic binaries are more luminous in NIR as they host red giants. Although many symbiotic binaries emit soft X-rays, a small fraction emit hard X-rays with $\sim$10 keV plasma temperature (e.g., Smith et al. 2008). They show strong Fe features in X-rays (e.g.,Smith et al. 2008; Eze 2014) and do not show Brγ emission lines in NIR (Schmidt & Mikołajewska 2003). It is worth mentioning that some symbiotic binaries are actually discovered in the follow-up studies of newly discovered X-ray sources (van den Berg et al. 2006).

To compare these possible populations with class C sources, we added extinction curves of a hibernating CV, a pre-CV, and a symbiotic star in figure 8. We see that both the possible populations and the class C sources scatter between class A and B sources as a group. This suggests that at least some of the class C sources are either hibernating CVs, pre-CVs or symbiotic stars, having the intermediate HR between CVs and late-type stars.

4.3 Contributions to the GRXE

How much fractional contribution does each class make for the GRXE, especially in the Fe K band? To answer this question, we fitted the composite spectra in the 4–8 keV band phenomenologically using a power-law continuum plus a Gaussian line representing the Fe K-band emission. The free parameters are power-law index, normalization, the Gaussian line width, and normalization. The Gaussian line center was fixed at 6.7 keV. The result (table 7, figure 9) indicates that the class C sources contribute $\sim$56% of the Fe K-band emission of all the identified sources. It is thus possible that class C sources make an important contribution to the GRXE, especially at the Fe K band, however this cannot be confirmed with the data at hand, since the sources we selected for the NIR study are not uniformly distributed among the three classes.

5 Summary

We presented results of a NIR spectroscopic follow-up study of dim X-ray point sources constituting the GRXE in the two fields of the GP. The main results are summarized as follows.

1. Well-exposed K_s-band spectra were obtained from a total of 65 X-ray sources in the two fields

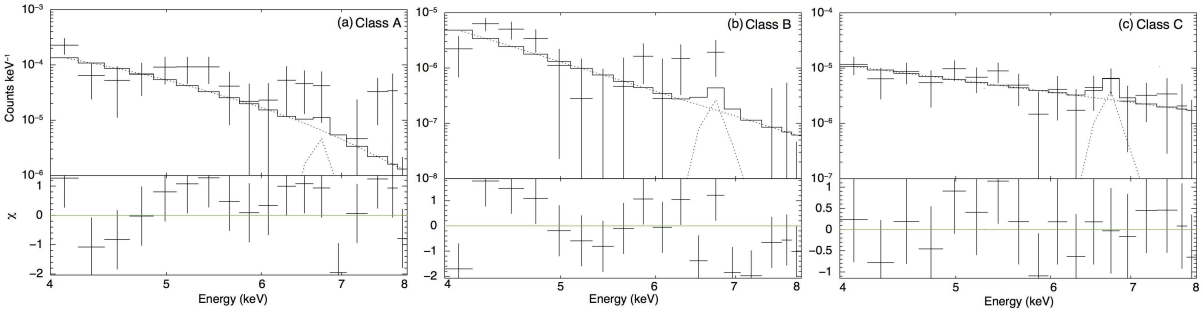

Fig. 9. Fe K feature in the composite spectra of the class (a) A, (b) B, and (c) C sources. The best-fit parameters are shown in table 7.

Table 7. Best-fit parameters for spectral fittings in 4–8 keV.

Class	$F_{\rm Gau}{}^{*}$ ($\rm ergs\ cm^{-2}\ s^{-1}$)	χ^2/d.o.f
A	$1.92^{+0.63}_{-0.41} \times 10^{-16}$	17.16/14
B	$1.60^{+0.52}_{-0.38} \times 10^{-17}$	23.68/15
C	$2.61^{+0.46}_{-0.25} \times 10^{-16}$	6.14/15

* Flux of the gaussian component.

studied by Chandra deep exposures.

2. Based on the NIR spectroscopic features and X-ray colors, we divided the sources into three categories: (A) hard X-ray sources with emission features in NIR such as H I, He I, and H_{II}, (B) soft X-ray sources with absorption features in NIR such as H I, Na I, Ca I, and CO band heads, and (C) hard X-ray sources with absorption features in NIR such as H I, Na I, Ca I, and CO bandheads.
3. We propose that class A and B sources are mainly comprised of CVs and X-ray active stars, whereas class C sources is presumably a different class distinctive from the two. We suggest that class C are binary systems hosting white dwarfs and late-type stars with low-level of accretion. Possible candidates of the class C sources are hibernating CVs, pre-CVs and symbiotic stars.
4. It is possible that this newly discovered class of sources contribute to a non-negligible fraction of the GRXE, especially in the Fe K band.

This work is based on data collected at Subaru Telescope operated by the National Astronomical Observatory of Japan and on observations made with an ESO Telescope at the La Silla Observatory under program ID 075.D-0767. IRAF is distributed by the National Optical Astronomy Observatories, which are operated by the Association of Universities for Research in Astronomy, Inc., under cooperative agreement with the National Science Foundation. This research has made use of SAOImage DS9, developed by Smithsonian Astrophysical Observatory. K. M. is financially supported by the University of Tokyo global COE program, the Hayakawa Satio Foundation by the

Astronomical Society of Japan, the Sasagawa Scientific Research Grant from The Japan Science Society, and the Hyogo Science and Technology Association. M. T is financially supported by MEXT/JSPS KAKENHI Grant Numbers 24105007 and 15H03642.

References

Ali, B., Carr, J. S., Depoy, D. L., Frogel, J. A., & Sellgren, K. 1995, AJ, 110, 2415

Allan, A., Hellier, C., & Beardmore, A. 1998, MNRAS, 295, 167

Anders, E. & Grevesse, N. 1989, Geochim. Cosmochim. Acta, 53, 197

Baskill, D. S., Wheatley, P. J., & Osborne, J. P. 2005, MNRAS, 357, 626

Bilíková, J., Chu, Y.-H., Gruendl, R. A., & Maddox, L. A. 2010a, AJ, 140, 1433

Bilíková, J., Chu, Y.-H., Gruendl, R. A., & Maddox, L. A. 2010b, AJ, 140, 1433

Cox, A. N. 2000, Allen's astrophysical quantities

Dempsey, R. C., Linsky, J. L., Fleming, T. A., & Schmitt, J. H. M. M. 1997, ApJ, 478, 358

Dempsey, R. C., Linsky, J. L., Schmitt, J. H. M. M., & Fleming, T. A. 1993, ApJ, 413, 333

Dhillon, V. S. & Marsh, T. R. 1995, MNRAS, 275, 89

Dhillon, V. S., Marsh, T. R., Duck, S. R., & Rosen, S. R. 1997, MNRAS, 285, 95

Ebisawa, K., Maeda, Y., Kaneda, H., & Yamauchi, S. 2001, Science, 293, 1633

Ebisawa, K., Tsujimoto, M., Paizis, A., et al. 2005, ApJ, 635, 214

Eze, R. N. C. 2014, MNRAS, 437, 857

Ezuka, H. & Ishida, M. 1999, ApJS, 120, 277

Grindlay, J. E., Hong, J., Zhao, P., et al. 2005, ApJ, 635, 920

Güdel, M., Linsky, J. L., Brown, A., & Nagase, F. 1999, ApJ, 511, 405

Hong, J. 2012, MNRAS, 427, 1633

Howell, S. B., Harrison, T. E., Szkody, P., & Silvestri, N. M. 2010, AJ, 139, 1771

Ichikawa, T., Suzuki, R., Tokoku, C., et al. 2006, in Presented at the Society of Photo-Optical Instrumentation Engineers (SPIE) Conference, Vol. 6269, Society of Photo-Optical Instrumentation Engineers (SPIE) Conference Series

Ishida, M., Matsuzaki, K., Fujimoto, R., Mukai, K., & Osborne, J. P. 1997, MNRAS, 287, 651

Koyama, K., Makishima, K., Tanaka, Y., & Tsunemi, H. 1986, PASJ, 38, 121

Laycock, S., Grindlay, J., van den Berg, M., et al. 2005, ApJL, 634, L53

Luna, G. J. M. & Sokoloski, J. L. 2007, ApJ, 671, 741

Matranga, M., Drake, J. J., Kashyap, V., & Steeghs, D. 2012, ApJ, 747, 132

Moorwood, A., Cuby, J.-G., & Lidman, C. 1998, The Messenger, 91, 9

Morihana, K. 2012, PASP, 124, 1132

Morihana, K., Tsujimoto, M., Yoshida, T., & Ebisawa, K. 2013, ApJ, 766, 14

Motch, C., Warwick, R., Cropper, M. S., et al. 2010, A&A, 523, A92

Muno, M. P., Baganoff, F. K., Bautz, M. W., et al. 2004, ApJ, 613, 326

Muno, M. P., Bauer, F. E., Baganoff, F. K., et al. 2009, ApJS, 181, 110

Nagashima, C., Nagayama, T., Nakajima, Y., et al. 1999, in Star Formation 1999, ed. T. Nakamoto, 397–398

Nagayama, T., Nagashima, C., Nakajima, Y., et al. 2003, in Society of Photo-Optical Instrumentation Engineers (SPIE) Conference Series, Vol. 4841, Society of Photo-Optical Instrumentation Engineers (SPIE) Conference Series, ed. M. Iye & A. F. M. Moorwood, 459–464

Nebot Gómez-Morán, A., Motch, C., Barcons, X., et al. 2013, A&A, 553, A12

Nucita, A. A., Maiolo, B. M. T., Carpano, S., et al. 2009, A&A, 504, 973

Pandey, J. C. & Singh, K. P. 2008, MNRAS, 387, 1627

Pandey, J. C. & Singh, K. P. 2012, MNRAS, 419, 1219

Rayner, J. T., Cushing, M. C., & Vacca, W. D. 2009, ApJS, 185, 289

Revnivtsev, M., Sazonov, S., Churazov, E., et al. 2009, Nature, 458, 1142

Revnivtsev, M., Sazonov, S., Forman, W., Churazov, E., & Sunyaev, R. 2011, MNRAS, 414, 495

Revnivtsev, M., Sazonov, S., Gilfanov, M., Churazov, E., & Sunyaev, R. 2006, A&A, 452, 169

Ribeiro, T., Baptista, R., Kafka, S., et al. 2013, A&A, 556, A34

Ritter, H. & Kolb, U. 2003, A&A, 404, 301

Schmidt, M. R. & Mikołajewska, J. 2003, in Astronomical Society of the Pacific Conference Series, Vol. 303, Symbiotic Stars Probing Stellar Evolution, ed. R. L. M. Corradi, J. Mikolajewska, & T. J. Mahoney, 163

Servillat, M., Grindlay, J., van den Berg, M., et al. 2012, ApJ, 748, 32

Smith, R. K., Brickhouse, N. S., Liedahl, D. A., & Raymond, J. C. 2001, ApJL, 556, L91

Smith, R. K., Mushotzky, R., Mukai, K., et al. 2008, PASJ, 60, 43

Tarenghi, M. & Wilson, R. N. 1989, in Society of Photo-Optical Instrumentation Engineers (SPIE) Conference Series, Vol. 1114, Society of Photo-Optical Instrumentation Engineers (SPIE) Conference Series, ed. F. J. Roddier, 302–313

van den Berg, M., Grindlay, J., Laycock, S., et al. 2006, ApJL, 647, L135

van den Berg, M., Hong, J. S., & Grindlay, J. E. 2009, ApJ, 700, 1702

van den Berg, M., Penner, K., Hong, J., et al. 2012, ApJ, 748, 31

Warwick, R. S., Turner, M. J. L., Watson, M. G., & Willingale, R. 1985, Nature, 317, 218

Weisskopf, M. C., Brinkman, B., Canizares, C., et al. 2002, PASP, 114, 1

Wilms, J., Allen, A., & McCray, R. 2000, ApJ, 542, 914

Worrall, D. M., Marshall, F. E., Boldt, E. A., & Swank, J. H. 1982, ApJ, 255, 111